Dispersion strengthening in vanadium microalloyed steels processed by simulated thin slab casting and direct charging.

Part 2 - chemical characterisation of dispersion strengthening precipitates

J.A. Wilson, A.J. Craven, Y. Li[*+] and T.N. Baker[*]

Department of Physics and Astronomy, University of Glasgow, Glasgow, G12 8QQ, Scotland, UK

[*]Metallurgy and Materials Engineering Group, Department of Mechanical Engineering, University of Strathclyde, Glasgow G1 1XJ, Scotland, UK.

+ Now at Vanitec, Winterton House, High Street Westerham, Kent TN16 1AQ. UK

Keywords:

High strength low alloy (HSLA) steel
Analytical electron microscopy
Electron energy loss spectroscopy
Precipitation
Thin slab direct charged process

Author for correspondence

Dr J A Wilson,
Department of Physics and Astronomy,
University of Glasgow,
Glasgow G12 8QQ,
Scotland, UK.

Phone **+44 (0)141 339 8855 ext.0853**

FAX **+44 (0)141 330 4464**

e-mail **j.wilson@physics.gla.ac.uk**

Abstract

The composition of the sub-15 nm particles in six related vanadium high strength low alloy steels, made by simulated thin slab direct charged casting, has been determined using electron energy loss spectroscopy (EELS). Such particles are considered to be responsible for dispersion hardening. For the first time, particles down to 4 nm in size have had their composition fully determined. In all the steels, the particles were nitrogen and vanadium rich and possibly slightly sub-stoichiometric carbonitrides. Equilibrium thermodynamics predicted much higher carbon to metal atomic ratios than observed in all cases so that kinetics and mechanical deformation clearly control the precipitation process. Thus it is important to formulate the steel with this in mind.

Introduction

Thin slab continuous casting followed by direct charging into an equalisation furnace has the potential to replace the traditional thick slab casting process for the production of thin sheet high strength low alloy (HSLA) steel. The new process provides significant reductions in capital costs, plant size and energy consumption whilst allowing rapid response to changes in demand with regard to steel compositions. [1,2] Furthermore, the use of electric arc furnaces enhances the ability to recycle scrap steel and reduces emissions from the plant. [3] Thus, both economically and environmentally, the direct charged thin slab (DCTS) process offers very significant benefits over the conventional process. [4]

However, changes in thermomechanical processing conditions result in differences in the evolution of steel's microstructure, which in turn affect its mechanical properties [5,6,7]. In thin slab continuous casting, steels no longer undergo the $\gamma \rightarrow \alpha \rightarrow \gamma$ phase transitions prior to equalisation and rolling as the slab is not first cooled to ambient temperature. Thin slabs are also subject to increased cooling rates and reduced mechanical deformation. Hence, if the new process is to be optimised, the evolution of the microstructure must be characterised. This is done using a simulated production process which allows samples to be taken at key processing points in a way that is not possible on a full-scale production mill. For example, in this project samples of the steel were water quenched following casting, equalization, four rolling passes and the final product. Whilst previous work has focused upon samples taken during the earlier stages of processing, [6, 8-11] here we are concerned solely with the sub-15nm particles which form in the final product. Part 1 of this paper, is concerned

with the effect dispersion strengthening vanadium precipitates have on the mechanical properties and microstructure of TSDC microalloyed vanadium steels. The thermodynamics and kinetics of preciptate formation is also considered in greater detail. Here, in part 2, we discuss their elemental composition, placing the results in the context of our earlier work. A preliminary report from this study has been given.[12]

The larger precipitates, which form in the early stages of processing, can act both beneficially, providing grain refinement, or deleteriously, prematurely removing alloying elements from the melt and thereby inhibiting the subsequent formation of dispersion strengthening precipitates. Those present after casting were plates, dendrites, complexes and irregularly shaped particles. Those present after equalization were cuboids and cruciforms, the cruciforms being observed only when Ti was added as a microalloying element[10]. Of these precipitates, the V based carbonitrides were actually effectively nitrides with very little carbon content. They would persist and grow through subsequent processing stages, becoming increasingly V rich thereby depleting bulk N and V levels before the fine dispersion hardening particles could form.

Theoretical equilibrium compositions of the small dispersion hardening particles, obtained using ChemSage software, predicted that they would be carbonitrides with a significant carbon content. Similar results were obtained by Langeborg *et al*. using the Thermo-Calc software package. [13] There are many references in the literature describing the dispersion hardening particles in vanadium steels as carbonitrides [e.g.

[14-21]. However, there are few actual detailed determinations of the compositions of such small particles and this is the area we address here.

The principal method of compositional analysis used was electron energy loss spectroscopy (EELS) [22] performed in a scanning transmission electron microscope (STEM). The particles were extracted onto amorphous carbon (*a-C*) films. This has a number of advantages. It removes the large amount of ferromagnetic matrix, which otherwise severely perturbs the optics of the objective lens. It also removes the diffraction contrast from the iron matrix and makes even the smallest particles clearly visible in an annular dark field (ADF) image. Most important for this study, it removes the large contribution to the background in the EELS spectrum that would have come from the matrix surrounding a small particle if studied in a thin foil specimen. The background from *a-C* films is also considerably lower than that from alternative films such as Al, amorphous Al_2O_3 and amorphous Si that have been used by other workers. [23-26] However, the major disadvantage of the use of *a-C* is that the contribution of the *a-C* to the C K-edge dominates that from the carbon in the particle (*c-C*) in the as-prepared replicas, preventing determination of the C content of particles.

A technique has been developed in which a plasma cleaner is used to thin the *a-C* films from under the particles so that they may be found overhanging cracks and holes. [27] The thinning process reduces the contribution from the *a-C* to a level at which it can be separated from the *c-C* contribution from the particle using the electron energy loss near edge structure (ELNES). In most cases the technique has

been found to cause little or no oxidation enabling a complete elemental composition to be obtained even for the smallest particles.

Experimental techniques

Production of the steels

The work was undertaken on six low carbon steels (~0.06wt%) each containing ~0.1wt%V. Steel **V** was the base-line steel with ~0.007wt%N. Steel **V-N** had an increased N level of ~0.02wt%. Steel **V-Ti** had ~0.008wt%Ti and ~0.02wt%N. The three final steels had ~0.01wt%N with Steel **V-Nb** having ~0.04wt%Nb, Steel **V-Nb-Ti** having ~0.04wt%Nb and ~0.008wt%Ti and Steel **V-Zr** having ~0.008wt%Zr. In addition, the steels typically contained the following levels (in wt%) of other elements Si (0.4), Mn (1.5), P (0.015), S (0.005), Cr (0.08), Mo (0.02), Ni (0.07), Al (0.025), B (<0.0005), Cu (0.07), O (0.007). Of these additional elements, Cr is found in the particles of interest. Even in the steels to which Ti was not added deliberately as a microalloying element, it was found in the particles formed during the earlier stages of the processing, presumably due to its presence at low level in the feedstock. However, unless Ti was added deliberately, no Ti was found in the sub-15nm particles in the final product.

The simulated thin slab cast production was performed at the Corus Swinden Technology Centre and is discussed in more detail in part 1 of this paper. In summary,

the steels were cast into three moulds before being hot stripped and transferred directly to an equalising furnace set at one of three equalisation temperatures (1050°C, 1100°C or 1200°C) where they were held for 30-60 minutes prior to rolling. Finish rolling temperatures varied from 880°C to 850°C. After rolling, the strip was cooled under water sprays to simulate run-out table cooling. The target for the end cool temperature of the strip was in the range 550-650°C but occasionally process difficulties were encountered which took it out of this range. Following cooling, the strips were immediately put into a furnace at 600°C and slow cooled to simulate coiling.

Table 1 gives values of equalisation and end cool temperatures of the samples reported here. In one case, samples with the same equalisation temperature but different end cool temperatures were studied. The concentrations of the relevant microalloying elements (V, Ti, Cr, Zr, Nb) are given as atomic ratios to their sum, *S,* since this is helpful in discussing the results The atomic ratios *N/S* and *N/V* are also given. It can be seen that in no case is there sufficient nitrogen to form stoichiometric nitrides with the metallic microalloying elements indicating that the steels are formulated on the assumption that the small particles will have a significant carbon content, as predicted by equilibrium thermodynamics.

Analysis of the particles

Extraction replicas were prepared by polishing the fully processed steels, etching with 2% nital before evaporating a thin carbon film onto its surface. Following stripping

in 5% nital, the films were washed in methanol and distilled water before being deposited onto Cu mesh grids.

The support film was thinned using a Fischione model 1020 plasma cleaner. The plasma cleaner operates in an inductively coupled mode which produces relatively low energy ions (20-40V). At these energies, sputtering of the specimen is kept to a minimum whilst carbonaceous material reacts with the activated oxygen to produce CO_2, CO and H_2O. [28] The gas used was 25% O_2, 75% Ar, as recommended by Fischione. In order to analyse the smallest particles, it is important that the side of the replica on which they lie is blanked otherwise "pedestals" of *a-C* are left underneath the particles. Details of the procedure can be found in reference. [27]

EELS measurements and annular dark field (ADF) imaging were performed using a VG Microscopes HB5 fitted with a Gatan Model 666 PEELS spectrometer. The microscope was operated at 100keV with convergence and collection semi-angles of 8 and 12.5 mrad respectively. Core loss edges were recorded using single acquisitions of 4 seconds. Low loss spectra were recorded from a sequence of 100 acquisitions, each of 40ms. A synchronised fast beam blank [29] ensured that the beam was incident on the detector for only 500 μs during each 40 ms acquisition, thereby preventing saturation by the zero loss peak. Dark currents were subtracted from the low loss and core loss spectra. The background under a group of overlapping edges was subtracted by extrapolation the function AE^{-r} in a region prior to the first edge. [22] Here, *A* and *r* are fitting parameters and *E* is the energy loss. Fourier ratio deconvolution was performed on core loss edges [22], which were also sharpened to

remove broadening due to point spread function of the detector. All these procedures used the routines in the Gatan EL/P software. Overlapping edges were then separated by fitting an appropriate edge shape to the non-overlapped portion of the first edge and subtracting it to extract the higher lying edge. In the case of the overlap of the N K-edge and Ti $L_{2,3}$-edges, the N K-edge was fitted with the N K-edge from a CrN standard. In the case of the overlap of the Zr $M_{4,5}$- or Nb $M_{4,5}$-edges and the C K-edge, the $M_{4,5}$-edges from the corresponding nitride were used. In the case of the overlap of the V $L_{2,3}$-edges and the O K-edge, the V $L_{2,3}$-edges from an unoxidised VN standard were used.

The relative proportions of metallic and non-metallic elements within particles were calculated by comparing their edge intensities with those from standard samples such as VN, TiN, TiC, NbN, NbC, ZrN and ZrC. For example, to calculate the N:V ratio of a particle, the total number of counts in a 40 eV windows over the N edge (I_{Nppt}) and the V $L_{2,3}$-edge (I_{Vppt}) are measured. Exactly the same procedure is used for the spectrum from the standard to obtain I_{Nst} and I_{Vst}. The N:V atomic ratio for the particle is then given by $(I_{Nppt}/I_{Vppt})/(I_{Nst}/I_{Vst})$.

For the metallic elements and N, this procedure is relatively straightforward and can be performed without the need for thinning of the support film. However, determination of the carbon content of a particle is complicated by the presence of the contribution from the *a-C* in the support film. For relatively large particles, it is possible to find a few of them overhanging cracks in the as-prepared replica. However, for the sub-15 nm particles of interest here, it is virtually impossible to find

them in this condition. An earlier paper [27] clearly demonstrates the use of a plasma cleaner to reduce the *a*-C to the level at which its contribution to the C K-edge is similar to that from the carbon in the crystalline precipitate (*c*-*C*). At this level, the difference in shapes of the C K-edges from *a*-*C* and *c*-*C* allow the amount of *c*-*C* in the spectrum to be determined. The C and N K-edge shapes are only slightly modified if V is replaced by Ti or Cr and so the same C K-edge shape can be used for steels containing these elements [30, 31] However, the changes in shape are much more significant if V is replaced by Nb or Zr and so, in principle, a different C K-edge shape should be used in the steels to which Nb or Zr has been added. [30, 31] However, Nb or Zr is only present at a relatively low concentration in the small particles of interest here and the shape of the N K-edge is hardly affected. Hence, it was only necessary to use one shape for the C K-edge in this work.

It is also necessary to determine if there is any O in the particle. This may result from the relatively high oxygen level present in an air melted laboratory steel, although the composition is such that any such oxygen ought to be taken up by elements such as Al. Alternatively, it might occur from exposure to the oxidising environments found in the Nital etch, the atmosphere and the plasma cleaner. Contributions to the O K-edge in the spectra from these small particles were found to come from two sources, the O in particle itself (*c*-*O*) and the O in the SiO_x formed by a low level of Si in the *a*-*C* support film. This Si is concentrated by the plasma ashing effect in which elements that form non-volatile oxides are retained in the film while those with volatile oxides are removed. The two contributions can be separated by their ELNES [27] in a similar manner to the separation of the two contributions to the C K-edge. This procedure results in a relatively high fractional

error in the *c-O/M* ratio. For example, if *c-O/M* is found to be 0.1 for a 10 nm particle, the fractional error could be as high as 30%. However, the absolute values found for *c-O/M* are typically small and so the absolute error is small. In what follows, the results are given for the particle compositions after the C and O contributions from the support film have been removed.

Results and Discussion

The particle composition versus temperature was modelled under equilibrium conditions for the target compositions of the steels using the ChemSage thermodynamic software package as described in more detail in part 1 of this paper. Examples of non-metal to metal ratios predicted for particles in Steels V and V-Ti are provided in Fig.1. A brief summary of the modelling results is provided in the paragraph below.

At temperatures above the $\gamma \rightarrow \alpha$ transition, precipitates formed in steels V, V-N and V-Ti particles are predicted to be stoichiometric nitrides. In the case of Steel V-Nb they were predicted to contain some carbon with the *C/M* ratio increasing from 0.15 to 0.25 as the temperature falls from the solution temperature to the $\gamma \rightarrow \alpha$ transition. Over the same temperature range the vacancy to metal ratio rises from 0 to ~0.04 in this steel. The calculations for Steel V-Nb-Ti give similar results. Similar calculations show that the *V/M* ratio increases markedly on cooling over this temperature range when microalloying elements other than V are present. These predictions are consistent with the experimental observations on the larger particles reported elsewhere [8,10,,11]. Below the $\gamma \rightarrow \alpha$ transition temperature, a sharp rise in the C

content is predicted. With the exception of Steel V-Ti, the particles are all predicted to have *C*/*M* of ~0.5 and (*C*+*N*)/*M* of ~0.85 at the target end cool temperature of 600°C, i.e. carbon-rich, slightly sub-stoichiometric carbo-nitrides. Even in Steel V-Ti, the particles are predicted to have *C*/*M* of ~0.3 and (*C*+*N*)/*M* of ~0.89. Where other microalloying elements are present, the *V*/*M* ratio is predicted to rise to between 0.8 and 0.9 at 600°C.

Fig. 2 shows all the values of *N*/*M* determined from particles in samples of Steels V, V-N and V-Ti equalised at 1100°C. As no *C* analysis is presented in this figure these data include points from as-prepared replicas, replicas thinned from both sides and replicas thinned from one side. Results from each technique are plotted separately and a linear trend line is plotted to indicate any effect of particle size. The time needed to thin a particular replica for analysis was determined both by its original thickness and whether the thinning is single or doubled sided. Fig. 3 summarizes the average *N*/*M* for each steel and thinning technique presented in Fig. 2. Fig. 4 provides the complete elemental analyses from Steel V-N equalised at 1100°C obtained using the single sided thinning technique (Figs. 2b and 2c). The results include 3 particles from the steel sample with the low end cool temperature (511°C) and 19 particles from three separate areas of a replica from the steel sample with the high end cool temperature (720°C). Fig. 4a is a cumulative bar chart of the values of *N/M*, *c-C/M* and *c-O/M*. Fig. 4b gives the corresponding values of *V/M* and *Cr/M*. Here the total height of the bars is unity since the particles contain only V and Cr as the alloying metals.

The careful combined analysis of Figs. 2 to 4 provides a wealth of information concerning the composition of the precipitates, the quality of the analysis and the effects of sample preparation.

Firstly, it is worth noting that, with the exception of one particle, the precipitates from steel V-N in Fig. 2b appear to form a set of stoichiometric nitrides. This suggests electron beam induced loss of nitrogen is not a problem here (a fact also confirmed through making repeated measurements on individual precipitates). Additionally, the degree of scatter suggests a random error ~0.1, which could be taken as a reasonable upper limit on the processing errors. More generally, the average values of *N/M* in Fig. 2 a-d were consistently higher than those predicted by Chemsage at the target end cool temperature.

It is clear from Fig. 4 that the values of *c-C/M* are all low for both end cool temperatures, ranging from 0.02 to 0.14 with a mean of 0.056. Areas 2, 3 and 4 are just different grid squares on the same replica prepared from the steel with the end cool temperature of 720^{o}C. As such, these areas are only a few hundred microns apart in the steel itself. The particles in area 2 have higher values of Cr/M than the typical values in areas 3 and 4. Thus, significant microsegregation of alloying additions occurs on this scale.

These microsegregation effects are also seen in the larger particles. For example, cruciforms were found with the arms Ti rich relative to the centre and vice versa. [10] Such microsegregation is likely to be due either to dendritic growth during the

relatively rapid solidification or to depletion of alloying elements by growth of large particles in earlier stages of the processing.

Fig. 3 shows that there is a difference of ~0.16 between the average *N*/*M* values for precipitates on unthinned replicas and those on replicas thinned from one side. This seems to show that plasma thinning is modifying the composition of the precipitates either by oxidation or sputtering of light elements. However, a number of details in Figs. 2 to 4 suggest that this conclusion may be too simplistic.

If the plasma thinning were responsible for the change in composition three consequences should be observed. The first consequence is that one would expect *N*/*M* to decrease with particle size as modification of the particle composition would be limited to its surface. There is some evidence for this from the trend lines in Fig. 2 but there is also an enormous scatter in the values and even one data set which has a negative slope. The dashed trend line in Fig. 2b is unreliable as it's dominated by the single highly oxidised particle at the left hand side of Fig. 4b.

The second consequence would be that one would expect the effects of double sided thinning to be more severe than those of single sided thinning since the particles should be protected from the plasma until the removal of the last shreds of *a*-*C* below them. Figs. 2a and d show that double sided thinning tends to have a smaller effect than single sided thinning but this may be due to shorter time required.

The third consequence would be that if the mechanism for modifying the particle composition was oxidation by excited oxygen, as proposed for the carbon removal [28] one would expect a degree of uniformity in oxidation of precipitates of a given size on a given replica. Fig. 4 clearly shows that different particles in the same area and groups of particles in different areas show different degrees of oxidation and similar results were obtained from the other steels

Thus there is some uncertainty in the mechanism and degree of particle modification. However, Fig. 3 can be used to put limits on the change of *N/M* ratio. The minimum value is that given by the analysis of the particles on replicas thinned from one side. The maximum value is 0.16 higher than this.

No equivalent data are available to check for an effect of the plasma cleaner on the *c-C/M* ratio. Here it is assumed that *C* and *N* will be lost at the same rate. Even if there is a moderate difference in the rates of loss, the fact that *c-C/M* is low will mean that the absolute error will be small. Since the drop in the value of *N/M* is from an average value of ~1.0 for the particles in Steel V-N Fig. 3, the low value of *c-C/M* remains valid for these particles. With the exception of the Nb containing steels, similar low values of *c-C/M* were seen for the other steels. In Steel V-Nb, 1 out of 7 particles was a carbide with no nitrogen content but the others had values of *c-C/M* comparable with those of Steel V-N. The results for particles from two areas of a replica from Steel V-Nb-Ti, thinned from one side, are shown in Fig. 5. Here, the average value of *c-C/M* of 0.21 is much higher. Assuming *c-C* and *N* are removed at the same rate, the change in *(c-C+N)/M* will be 0.16 as for the other particles. Even

if they are removed at different rates, the change will be close to 0.16 because the particle is still N-rich.

Within these limits, the results from the six steels can be considered. Fig. 6 shows the values of the average particle compositions measured from nine processed steel samples using replicas thinned from one side. These values are plotted as a function of the ratio of the nitrogen to microalloying elements in the steels (*N/S*). The *N/M* ratios for steels V-N, V-Ti, V-Nb and V-Zr are all in the region of 0.8. Those for Steels V and V-Nb-Ti are ~0.65. The values of (*N*+*c*-*C*)/*M* lie between 0.83 and 0.89 for all steels except Steel V where it is only 0.71. If the *c*-*O* present is assumed to result from the conversion of VN to V_2O_5, as seen in VN powder, then the N content should be increased by *c*-*O*/2.5. The plot of (*N*+*c*-*C*+*c*-*O*/2.5)/*M* is little different to that of (*N*+*c*-*C*)/*M* showing that oxidation does not correct any modification of the precipitate composition from the thinning process. Thus the plot of (*N*+*c*-*C*)/*M* represents the lower limit for the value of the non-metal to metal ratio in the precipitates. Adding 0.16 to this value give the upper limit, also plotted on Fig. 6.

Fig. 7 shows the average metal fractions in the small particles in the six steels. In the Steels V-Nb, V-Ti and V-Nb-Ti, mixed transition metal particles were present. It is of interest to note that while Cr is a trace element in all the steels, it is present in significant quantities in the small vanadium containing particles in Steels V and V-N. Goldschmidt considers that Cr will form a complete solid solution with V as nitride and carbide [32].

If the values on the lower limit of (N+c-C)/M in Fig. 6 are compared with their corresponding ChemSage predictions, it is found that the values match somewhere in the temperature range 600^{o}C to 750^{o}C for Steels V-N, V-Ti, V Nb and V-Nb-Ti, but that the value for Steel V is below the predicted value at 600^{o}C. The differences between the curves (N+c-C)/M and N/M in Fig. 6 (i.e. the values c-C/M) for Steels V-N, V-Ti, V-Nb are ~0.05 while that for Steel V is 0.08 and that for Steel V-Nb-Ti is 0.21. Predicted values of c-C/M only match these values close to the γ to α transition temperature for Steels V, V-N and V-Ti and only well into the γ temperature range for Steels V-Nb (>1250^{o}C) and V-Nb-Ti (900^{o}C). However, it should be remembered that ChemSage predicts data for conditions of equilibrium, while the fast cooling rates experienced by the steels as the rolling process proceeds would be expected to induce a supersaturated state with a corresponding departure from equilibrium.

The estimated maximum values of (N+c-C)/M in Fig. 6 are ~1.0 except for Steel V where it is ~0.9. These values are close to those predicted near the γ to α transition temperature. Thus one interpretation of the results is that the precipitation of these small particles occurs close to the transition temperature, where both the c-C/M and the (N+c-C)/M values match the ChemSage predictions. This explanation requires that, once formed, the precipitates do not grow as the temperature falls otherwise the c-C content would increase either in an homogeneous fashion or with the growth of a carbon rich outer portion. This clearly does not happen in Steels V and V-N where the particles analysed on unthinned replicas show a N/M ratio approaching unity, as shown, for example, in Fig. 1. The bigger the particles, the closer to unity the values are. These are the particles where the extra growth would have been expected to be

C-rich. The similarity of the results from other steels in Fig. 6 suggests strongly that similar behaviour is present in all steels. This agrees with the discussion in part 1 of this paper, where a lack of coarsening is noted.

Comparing the results from Steel V-N with different thermomechanical treatments shows that little difference is seen between the steels with equalisation temperatures of 1200°C and 1100°C while there may be a small effect from end cool temperatures of 511°C and 720°C. Equalisation at 1050°C appears to produce a reduction in the value of *N/M* which is compensated by an increase in *c-C/M*. This occurs despite this sample having the highest ratio of N to microalloying elements (*N/S*) (Table 1). However, with an equalisation temperature of 1050°C, nitrogen starts to precipitate out at the equalisation stage, both as vanadium based nitrides and also as aluminium nitride [11]. Hence, the amount of N relative to V available for the final stage of precipitation is lowered. If significant precipitation occurs during the earlier stages of the process, then the effective value of *N/V* for atoms still in solution at the start of the final pass will move towards that in Steel V equalised at 1100°C, where a low average value of N/V is also observed for these small particles (Fig. 6).

In this particular chemical analysis, the smallest particles found, which were considered to be responsible for dispersion strengthening, were ~4 nm in size, although a small number of sub-4 nm V-based precipitates were recorded using the Philips EM 440T at the University of Strathclyde (see part 1 of this paper). Had smaller V-based precipitates been present on the replicas analysed using the HB5, they would have been seen easily in the ADF image. SiO_x particles down to 2 nm in size on the thinned support film are clearly visible in such images. These particles

are formed from the small concentration of Si in the support film by the plasma "ashing" effect during the thinning process. Heavier V-based particles of this size would scatter more strongly and hence be more visible. Thus we conclude that there were very few, if any, particles smaller than 4 nm on the replicas. A number of studies in the literature have considered the same problems. [16,17] Both Siwecki *et al.* [16] and Houghton *et al*. [17] used carbon extraction replicas to obtain particle size distributions in V steels. While both claim that their lower size limit was 2 nm, very few data in this range are included in their distributions. On the other hand, Dunlop and Honeycombe [33] used foils to study V, Ti and V-Ti carbides and their distributions, obtained from dark field electron micrographs, contained significant numbers of particles around 2 nm in size. They compiled their distributions from 150-200 particle size measurements and claimed an accuracy of ±1 nm. The mean particle size was confirmed using the atom probe, which also provided a particle composition of (V, Ti)$C_{0.84}$ for the V-Ti steel. [34]

As pointed out by Siwecki *et al*. [16] in support of their choice of replicas rather than foils, the confusion due to strain fields in the latter could give rise to high levels of inaccuracy at small particle sizes. However, this did not appear to be a problem in the work of Dunlop and Honeycombe [33] mainly due to the very high particle volumes in their alloys. The only way to resolve this uncertainty is to make a future study of foil specimens. Preliminary work on foils taken from Steel V-N equalised at 1100^{o}C has found vanadium particles down to 1 nm in size but these are still N rich [35].

The results presented here appear at odds with the thermodynamic predictions and indeed much of the historical perception for vanadium microalloyed steels undergoing a decomposition to ferrite i.e. the available nitrogen should initially form a high nitrogen carbonitride [14, 15, 17-21]. When all the nitrogen is consumed, the remaining vanadium should theoretically combine with carbon. Siwecki *et al,* [16] showed by indirect means that this did not occur. The present work finds the same result by direct analysis of small particles. Part 1 of this paper discusses in detail the results of this EELS analysis in the context of various thermodynamic and kinetic models for precipitation. It is concluded that the nitride precipitates nucleate rapidly at high temperatures within the ferrite. The high cooling rate and rapidly decelerating kinetics specific to the TSDC process then prevent coarsening or further nucleation of more carbon-rich particles. The modelling approach which provides the best agreement with our experimental data is that of Roberts and Sandberg[35], following that of Woodhead[36].

Since the steels studied here were formulated on the assumption that the small particles in the final product would be the predicted C-rich carbonitrides, the N concentrations in the steels are too low to bring all the alloying elements out of solution as N-rich carbonitrides. In the light of these results, an increase in the N content of the steel seems to be indicated in order to make full use of the expensive alloying additions.

Conclusions

In this paper, a study of the complete elemental analyses obtained from dispersion strengthening particles as small as 4 nm is described for a number of related V steels following simulated TSDC processing.

The dispersion strengthening particles were essentially nitrides which, despite being exposed to oxidising environments at a number of stages in the specimen preparation, showed very little evidence of oxidation. The small amount of oxidation observed may have been a local effect on the specimen or even in the steel itself. Very few particles from the steel smaller than ~4nm in size were present on the extraction replicas although recent work on foils shows that they may be present in the bulk.[34]

When Ti and Nb are added as alloying elements, they appear in the small particles but the *V/M* atomic ratio is larger than in the larger particles formed at higher temperature earlier in the process. When Zr is added to the steel it does not appear in the dispersion strengthening particles. Cr, not added intentionally as an alloying element, is present in some of the particles in nearly all of the steels but the average value of *Cr/M* varies from steel to steel. No Ti appears in the dispersion strengthening particles unless added as an alloying element although it is found in larger particles as a result of the Ti content of the feedstock used.

For steels equalised at 1100^{o}C, the *N/M* atomic ratio in the particles is related to the average nitrogen to alloying element ratio, *N/S*, in the steel. *N/M* rises rapidly to a "saturation" value of ~0.8 as *N/S* rises. Lowering the end cool temperature from 720^{o}C to 511^{o}C in Steel V-N raises the average *N/M* ratio in the particles by ~0.1.

Only in Steel V-Ti is there clear evidence for an increase in *N/M* with particle size. In Steel V-N at the higher end cool temperature, there may be a similar but weaker trend. For Steels V-Nb, V-Nb-Ti and V-Zr, the data sets are too small to see a trend.

The (N+c-C)/M atomic ratio is in the range 0.85 to 1.0 for most of the steels with in reasonable agreement with the predictions of equilibrium thermodynamics. The exception is Steel V, the steel with the lowest *N/S* value, where (N+c-C)/M is between 0.65 and 0.9. The unexpectedly low *c-C/M* ratio observed is believed to be a result of the rapid cooling in the TSDC process (See paper 1).

Acknowledgements

The authors would like to thank the following: EPSRC, for financial support under grants GR/M22888 and GR/M22918; Corus Group PLC, for financial support and for supply of materials and characterisation; VANITEC, for financial support. They would also like to thank David Crowther and Bill Morrison of Corus Group PLC and Peter Mitchell of Vanitec for useful discussion and advice.

References

[1] R. Kaspar, N. Zentarat and J. C. Herman: Steel Research, 1994, **65**, 279-283.
[2] R. Kaspar and O. Pawelski: in Proceedings of the Int. Conf. METEC Congress, VDEH, Dusseldorf, Germany, 1994, 390-304.
[3] P.J. Lubensky , S.L. Wigman and D.J. Johnson: Proceedings of the Int. Conf. 'Microalloyed 95', 1995, 225-233 Pittsburgh (PA), Iron & Steel Soc.
[4] V. Leroy and J.C. Herman : Proceedings of the Int. Conf. 'Microalloying 95', 1995, 213-223 Pittsburgh (PA): Iron & Steel Soc.
[5] M. Korchynsky, Scandinavian Journal of Metallurgy 1998, **28**, 40-45
[6] D. N. Crowther, Y. Li, T.N. Baker, M.J.W. Green and P.S. Mitchell : in 'Proceedings of Int. Conf. Thermomechanical Processing of Steels.', 2000. 527-536 London: Institute of Materials.
[7] R. Priestner, Mat.Sci Forum 1998, **95,** 284-286.

[8] Y. Li, D.N. Crowther, J.A. Wilson, A.J. Craven, and T.N. Baker: IOP Conf Ser 2001, **168**,183-186.
[9] Y. Li, D.N. Crowther, P.S. Mitchell and T.N.Baker: ISIJ International 2002, 42, 636-644.
[10] T.N. Baker, Y. Li, J.A.Wilson , A.J. Craven, and D.N. Crowther: Materials Science and Technology 2004, **20**, 720-730.
[11] Y. Li, J.A.Wilson, D.N. Crowther, P.S. Mitchell, A.J. Craven and T.N. Baker: ISIJ International 2004, **44** ,1093-1102.
[12] [12] J.A. Wilson, A.J. Craven, Y. Li and T.N. Baker: IOP Conf Ser 2001, **168,** 187-190.
[13] R. Langeborg, T. Siwecki, S. Zajac and B. Hutchison: Scand. J Met. 1999, **28**, 186-241.
[14] H.A. Vogels, P. Konig and K-H. Piehl: Archiv. Eisenh. 1964, **35**, 339-351
[15] T.N. Baker: Metals Tech. 1974, **1**, 126-131.
[16] T. Siwecki, A. Sandberg, W. Roberts and R. Lagneborg: in 'Themomechanical Processing of Austenite' (Ed. A.J. deArdo, G. A. Ratz and P.J. Wray), Warrendale (PA): 163-194, 1982, Met. Soc. AIME.
[17] D.C. Houghton, G.C. Weatherly, and Embury JD: in 'Themomechanical Processing of Austenite' (Ed. A.J. deArdo, G. A. Ratz and P.J. Wray). Warrendale (PA): 267-292, 1982, Met. Soc. AIME.
[18] W. Roberts. : in 'HSLA Steels, Technology and Applications'(Ed. M. Korchynsky). 33-65, 1984, Metals Park (OH): ASM.
[19] J. Strid and K.E. Easterling: Acta Metall 1985, **33**, 2057-2074.
[20] F. Sun and W Cui : in 'HSLA Steels, Processing, Properties and Technology' Ed. G. Tither and S. Zhang). 43-50, 1992, Warrendale (PA): TMS.
[21] T. Gladman. : in 'HSLA Steels, Processing, Properties and Technology.' (Ed.G. Tither, and S. Zhang) 3-14, 1992, Warrendale (PA): TMS.
[22] R.F. Egerton RF. Electron Energy Loss Spectroscopy in the Electron Microscope, 2nd Edition, 1996, Plenum New York.
[23] Y. Ishiguro and K. Sato: Materials Transaction, JIM 1996, **37**, 643-649
[24] A.J. Garratt Reed In:, 'Quantitative Microanalysis with High Spatial Resolution' (Eds. Lorimer GW, Jacobs MH, Doig P), Book 277. London: The 165, 1981, Metals Society.
[25] S.P. Duckworth, A.J. Craven and T.N. Baker: IOP Conf. Ser. 1984, **68**, 339-342.
[26] C. P. Scott, D. Chaleix, P. Barges and V. Rebischung: Scripta Mater 2002, **47**, 845-849.
[27] J.A. Wilson and A.J. Craven: Ultramicroscopy 2003, **94**, 197-207.
[28] T.C. Isabell, P.E. Fischione, C. O'Keefe, M.U. Guruz and V.P. Dravid: Microsc. Microanal 1999, **5**, 126-135.
[29] A. J. Craven, J.A. Wilson, W.A.P. Nicholson: Ultramicroscopy 2002, **92**, 165-180.
[30] A .J. Craven and L. A. J. Garvie: Microsc. Microanal. Microstruct. 1995 , **6,** 89-98.
[31] A.J. Craven: J. Microsc. 1995, **180**, 250-262.
[32] H.J.Goldschmidt, Interstitial Alloys,1957, 238,Butterworths,London.
[32] G. L. Dunlop, R.W.K. Honeycombe: Met. Sci. 1978, **12**, 367-371.
[33] G. L. Dunlop and P.J. Turner: Met. Sci. 1975, **9**, 370-374.
[34] M. MacKenzie, C. Collins private communication.

[35] W.Roberts and A.Sandberg, Swedish Institute for Metals, Report No IM-1489, Stockholm, 1980.
[36] J.H.Woodhead, Proc.Seminar Vanadium in high strength steel, 3- 10,Chicago, 1979,Vanitec, London.

Steel	Equalisation temperature (^{o}C)	End cool temperature (^{o}C)	$\frac{N}{V}$	$\frac{N}{S}$	$\frac{V}{S}$	$\frac{Cr}{S}$	$\frac{Ti}{S}$	$\frac{Nb}{S}$	$\frac{Zr}{S}$
V	1100	603	0.25	0.13	0.53	0.47	0.001		
V-N	1100	511	0.69	0.33	0.48	0.52	0.001		
V-N	1100	720	0.62	0.35	0.56	0.44	0.001		
V-N	1050	602	0.76	0.40	0.53	0.47	0.002		
V-N	1200	250	0.62	0.35	0.56	0.44	0.001		
V-Ti	1100	537	0.73	0.39	0.53	0.42	0.051		
V-Nb	1100	647	0.36	0.19	0.54	0.38	0.002	0.080	
V-Nb-Ti	1100	603	0.33	0.17	0.52	0.37	0.040	0.077	
V-Zr	1100	592	0.36	0.20	0.54	0.43	0.002		0.027

Table 1 Equalisation temperature, end cool temperature and atomic fractions of the alloying elements in the steel samples studied. *S* is the sum of the microalloying elements (V, Ti, Cr, Nb or Zr) present in the steel. The concentrations were obtained from bulk analyses supplied by Corus Group PLC.

Figure Captions

Figure 1 Examples of equilibrium concentration versus temperature predicted by ChemSage for the target compositions of selected steels. Non-metal to metal ratios are shown for a) Steel V and b) Steel V-Ti. The dotted vertical line is the temperature predicted for the $\gamma \rightarrow \alpha$ phase transition of the matrix on cooling.

Figure 2 N/M atomic ratios for small precipitates in steels equalised at 1100^{o}C: a) Steel V; b) Steel V-N, lower end cool temperature; c) Steel V-N, higher end cool temperature; d) Steel V-Ti. Different marker types indicate groups of particles from replicas which have undergone different degrees of plasma processing. Lines of best fit have been fitted for each data set.

Figure 3 Average N/M ratios for small precipitates in steels V, V-N, and V-Ti. The letters H and L correspond to the steels with end cool temperatures of 720°C and 511°C respectively

Figure 4 a) Non-metal/metal ratios for small particles and b) metal ratios in Steel V-N. The particles in Area 1 are from a sample with an end cool temperature of 511°C whereas those in Areas 2, 3 and 4 are from a sample with an end cool temperature of 720°C.

Figure 5 Non-metal/metal ratios for small particles in Steel V-Nb-Ti.

Figure 6 Plot of the non-metal/metal atomic ratios in the small particles versus the nitrogen/metal atomic ratio in the steel, *N*/*S* (Table 2). All the steels were equalised at 1100^{o}C with an end cool temperature in the target range apart from V-N(H) and V-N(L) which have the high and low end cool temperatures respectively, and V-$N_{(1050)}$ and V-$N_{(1200)}$ which have equalisation temperatures of 1050^{o}C and 1200^{o}C respectively.

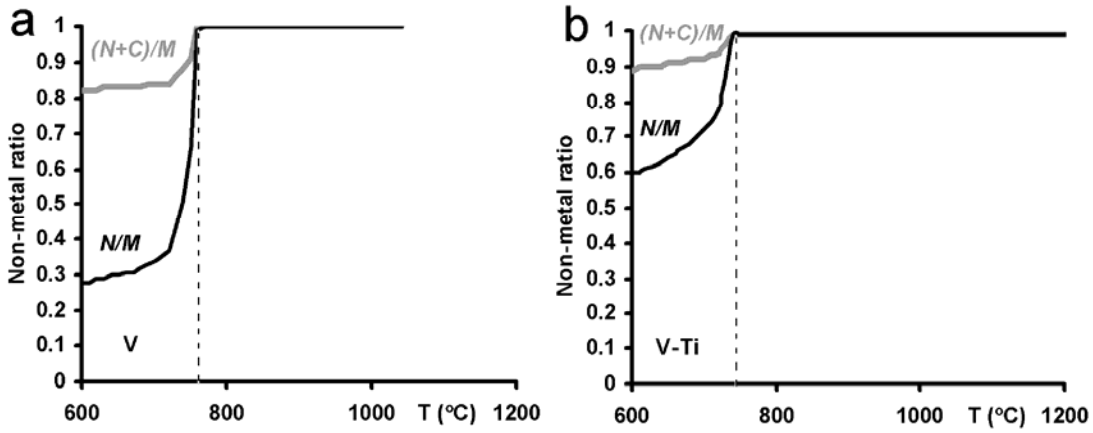

Fig 1

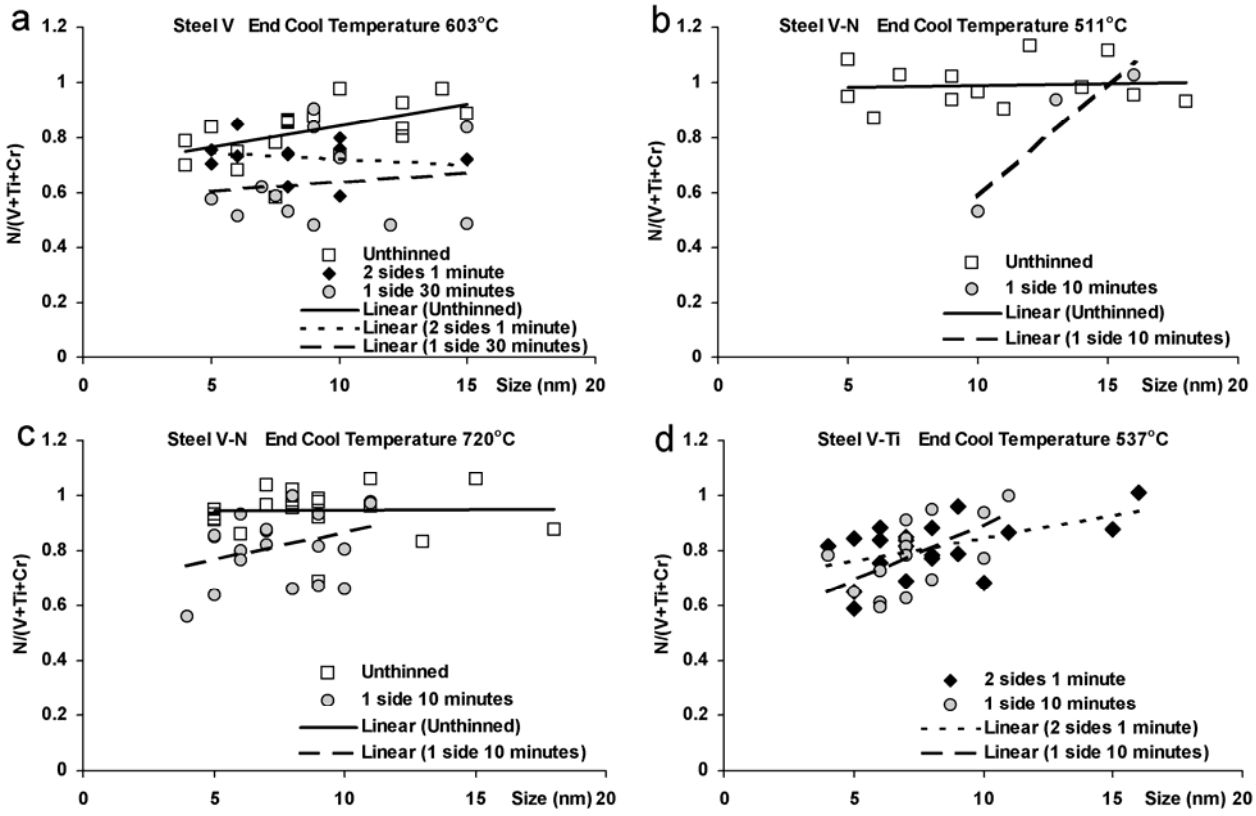
a
Steel V End Cool Temperature 603°C
N/(V+Ti+Cr)
Size (nm)
Unthinned
2 sides 1 minute
1 side 30 minutes
Linear (Unthinned)
Linear (2 sides 1 minute)
Linear (1 side 30 minutes)
b
Steel V-N End Cool Temperature 511°C
N/(V+Ti+Cr)
Size (nm)
Unthinned
1 side 10 minutes
Linear (Unthinned)
Linear (1 side 10 minutes)
c
Steel V-N End Cool Temperature 720°C
N/(V+Ti+Cr)
Size (nm)
Unthinned
1 side 10 minutes
Linear (Unthinned)
Linear (1 side 10 minutes)
d
Steel V-Ti End Cool Temperature 537°C
N/(V+Ti+Cr)
Size (nm)
2 sides 1 minute
1 side 10 minutes
Linear (2 sides 1 minute)
Linear (1 side 10 minutes)

Fig 2

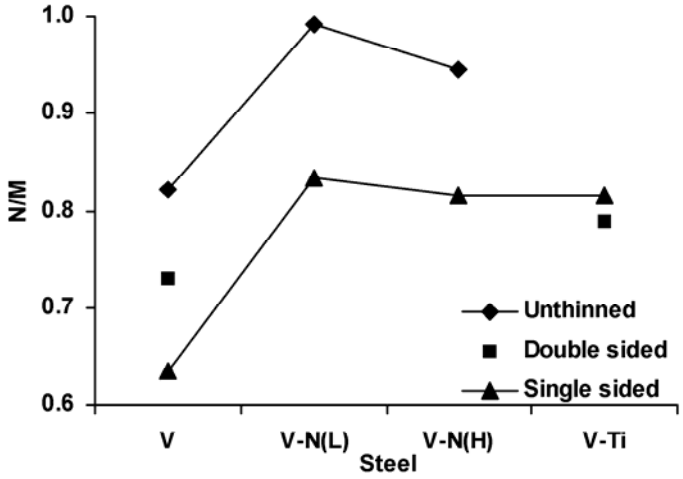
1.0
0.9
0.8
0.7
0.6
N/M
Unthinned
Double sided
Single sided
V
V-N(L)
V-N(H)
V-Ti
Steel

Fig 3

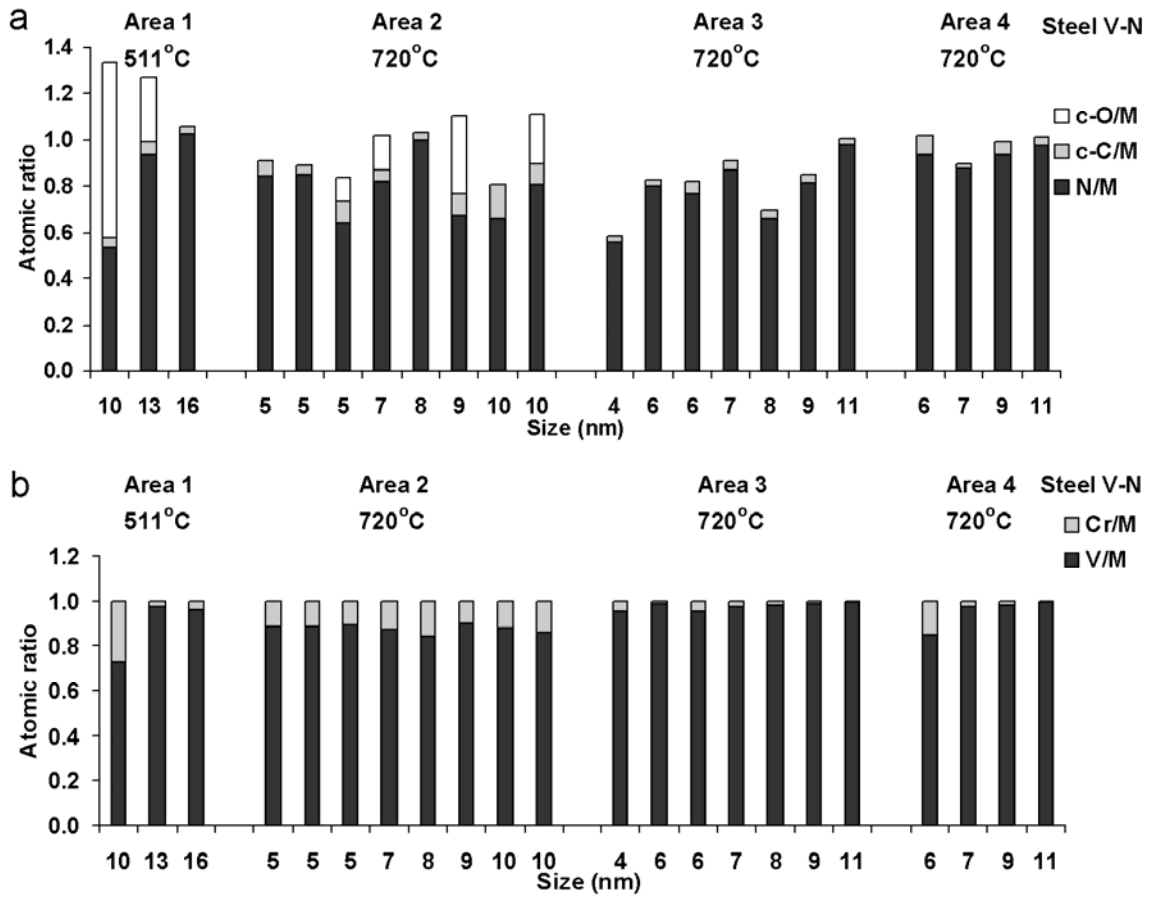
a
Area 1
511°C
Area 2
720°C
Area 3
720°C
Area 4
720°C
Steel V-N
c-O/M
c-C/M
N/M
Atomic ratio
1.4
1.2
1.0
0.8
0.6
0.4
0.2
0.0
10 13 16 5 5 5 7 8 9 10 10 4 6 6 7 8 9 11 6 7 9 11
Size (nm)
b
Area 1
511°C
Area 2
720°C
Area 3
720°C
Area 4
720°C
Steel V-N
Cr/M
V/M
Atomic ratio
1.2
1.0
0.8
0.6
0.4
0.2
0.0
10 13 16 5 5 5 7 8 9 10 10 4 6 6 7 8 9 11 6 7 9 11
Size (nm)

Fig 4

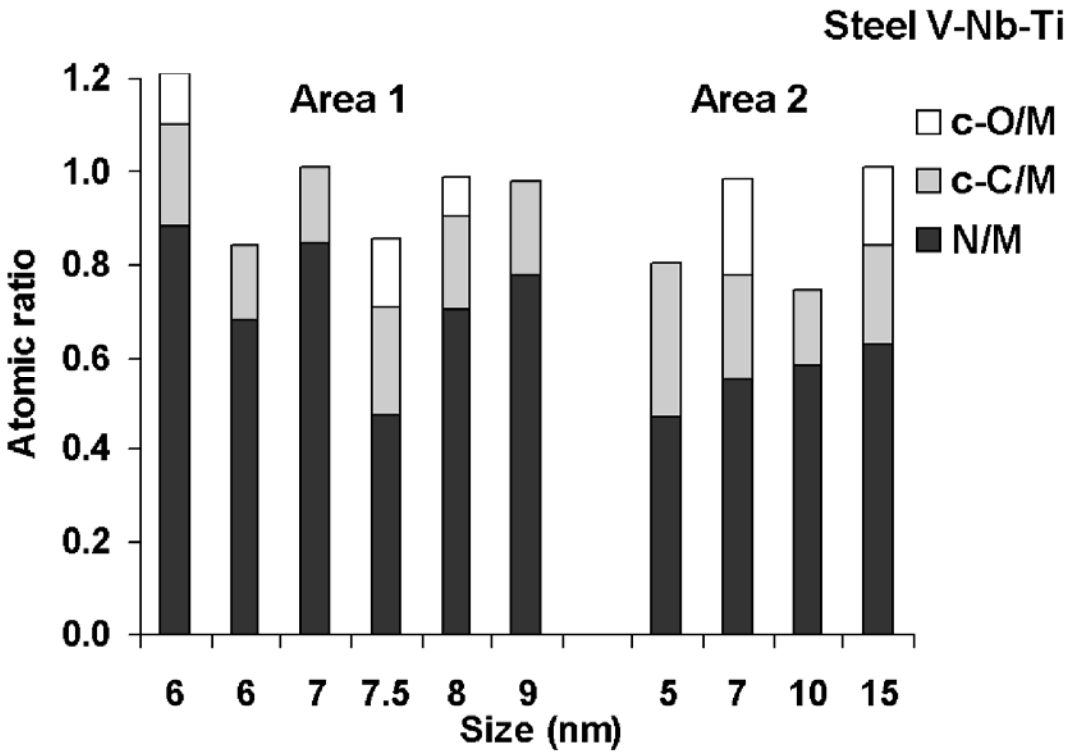
Steel V-Nb-Ti
Area 1
Area 2
c-O/M
c-C/M
N/M
Atomic ratio
1.2
1.0
0.8
0.6
0.4
0.2
0.0
6
6
7
7.5
8
9
5
7
10
15
Size (nm)

Fig 5

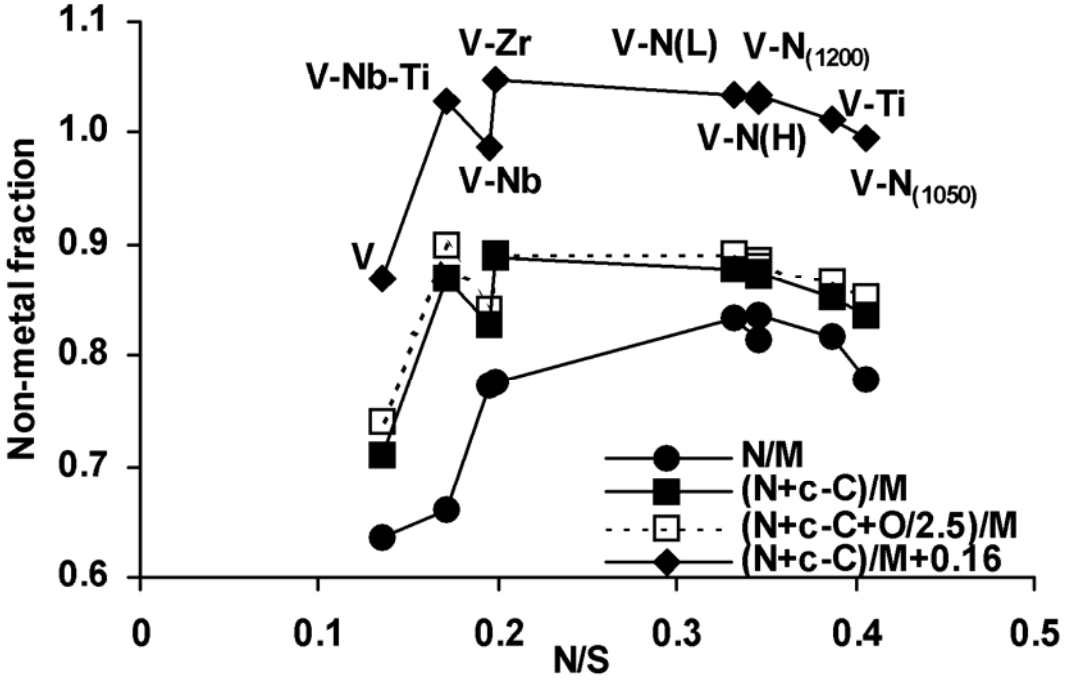
Non-metal fraction
1.1
1.0
0.9
0.8
0.7
0.6
0
0.1
0.2
0.3
0.4
0.5
N/S
V-Zr
V-N(L)
V-N(1200)
V-Nb-Ti
V-Ti
V-N(H)
V-Nb
V-N(1050)
V
N/M
(N+c-C)/M
(N+c-C+O/2.5)/M
(N+c-C)/M+0.16

Figure 6

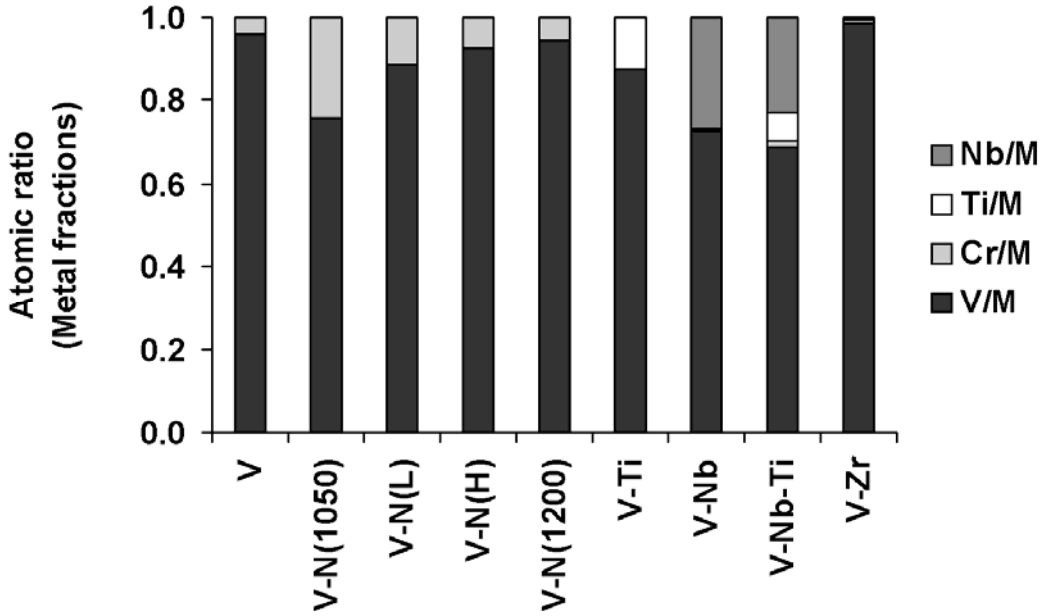
Atomic ratio
(Metal fractions)
1.0
0.8
0.6
0.4
0.2
0.0
V
V-N(1050)
V-N(L)
V-N(H)
V-N(1200)
V-Ti
V-Nb
V-Nb-Ti
V-Zr
Nb/M
Ti/M
Cr/M
V/M

Figure 7